

Chapter

NON-EQUILIBRIUM SEDIMENT TRANSPORT MODELING — FORMULATIONS AND CLOSURES

*Weiming Wu**

National Center for Computational Hydroscience and Engineering,
The University of Mississippi, MS 38677, USA

ABSTRACT

In this chapter, the general formulations, closure methods, and capabilities of the non-equilibrium sediment transport (NEST) modeling are comprehensively described. By integrating the 3-D model equations over the flow depth (or cross-section), the depth-averaged 2-D (or 1-D) flow, suspended-load, and bed-load transport equations are derived. As an alternative approach, the depth-averaged bed-material load transport equation is derived by combining the bed-load and suspended-load equations. The momentum and suspended-load dispersion terms can be combined with the turbulent stress/diffusion terms or convection terms, or evaluated using analytical models of secondary flow if available. The near-bed exchange fluxes are assumed proportional to the difference between the actual and capacity (equilibrium) concentrations and transport rates of sediment via the adaptation coefficient α and/or the adaptation length L . The temporal lag between flow and sediment transport is modeled by introducing the bed-load velocity and the correction factor β_s , which is the ratio of the depth-averaged velocities of suspended load and flow. Methods and guidance have been developed to determine the sediment velocity, adaptation length, and transport capacity. In the case of non-uniform sediments, the mixing layer concept is adopted for bed material sorting, and a correction factor is introduced in sediment transport capacity formulas to account for the hiding and exposure effect in the bed materials. Additionally, turbulence closure, bed roughness, sediment transport over steep slope, sediment entrainment near in-stream structures, and bank erosion are briefly discussed to close and enhance the model. Numerical methods often used to solve the flow and sediment transport equations are briefly summarized, and test cases are selected to demonstrate the capabilities of the NEST model.

Keywords: Adaptation length; non-equilibrium transport model; non-uniform sediments

* Email: wuwm@ncche.olemiss.edu

INTRODUCTION

Sediment transport processes in surface waters are among the most complex and least understood phenomena in nature. The early research methodologies were primarily based on field observations and laboratory experimentations. With the rapid advances of fundamental theories, numerical algorithms, and computer technologies, computational modeling has been more and more widely applied to solve many sedimentation engineering problems.

Many numerical models have been developed since 1950s. Most of the early models assume that bed load or total load is instantaneously in equilibrium at each computational node. Such models are referred to as equilibrium (or saturated, capacity) transport modeling approach (Thomas, 1982; Spasojevic and Holly, 1993). However, because of the dynamic nature (unsteadiness, non-uniformity) of surface water flows, sediment transport in nature is rarely in an equilibrium state. The assumption of local equilibrium need to be improved to take into account the non-equilibrium features of sediment transport. Therefore, non-equilibrium sediment transport (NEST) modeling has emerged in recent decades as a more realistic technology. This approach renounces the assumption of local equilibrium and solves the actual transport equations for bed and suspended loads; thus, it can describe the temporal and spatial lags between flow and sediment transport. Examples of NEST models with varying levels of complication have been reported by Han (1980), Bell and Sutherland (1983), Armanini and di Silvio (1988), Rahuel et al. (1989), and Wu et al. (2000a, 2004). To meet the needs of the more recent engineering practices, the NEST modeling have been further advanced and applied to simulate non-cohesive/cohesive sediment transport, local scour around in-stream structures, channel meandering, dam/levee breaching, sediment transport in vegetated channels, upland soil erosion, coastal sedimentation, etc.

The NEST modeling approach is introduced in two chapters. Its general formulations are presented in this chapter, including governing equations, numerical solution methods, and model closures. Presented in the next chapter are its extensions and applications in specific cases, such as rapidly-varying transient flows over movable beds, sediment transport in coastal waters and vegetated channels, and upland soil erosion. In each application area, test examples are selected to demonstrate the capabilities of the NEST modeling approach.

GOVERNING EQUATIONS

3-D Flow and Suspended-Load Transport Equations

The phenomena of flow and sediment transport in surface waters are characterized by turbulence, free-surface variation, bed change, phase interaction, etc. In order to model such complex processes, simplifications and assumptions are usually needed. At the present, most sediment transport models assume low sediment concentration, so that the hydrodynamics of the flow is not affected by sediment movements and the flow and sediment transport equations can be solved separately or decoupled. It is also assumed that the time scale of bed change is much larger than that of flow movement, so that in each time step the flow can be

calculated by assuming a “fixed” bed. Based on these assumptions, the 3-D flow field can be determined using the Reynolds-averaged continuity and Navier-Stokes equations given by Equations (1) and (2), where t is time, x_i is the i^{th} coordinate (x, y, z for $i=1,2,3$), u_i is the flow velocity component in the i^{th} coordinate direction, F_i includes the external forces per unit volume, including the gravity force, ρ is the flow density, p is the pressure, and τ_{ij} denotes the turbulent stresses, which are determined using a turbulence model.

$$\frac{\partial u_i}{\partial x_i} = 0 \quad (1)$$

$$\frac{\partial u_i}{\partial t} + \frac{\partial(u_i u_j)}{\partial x_j} = F_i - \frac{1}{\rho} \frac{\partial p}{\partial x_i} + \frac{1}{\rho} \frac{\partial \tau_{ij}}{\partial x_j} \quad (2)$$

For the shallow water flow, the pressure can be assumed to be hydrostatic, thus yielding the simplified 3-D governing equations as given by Equations (3), (4), and (5), where x and y are the horizontal Cartesian coordinates, z is the vertical coordinate, z_s is the water surface elevation, g is the gravitational acceleration, and f is the Coriolis coefficient.

$$\frac{\partial u}{\partial x} + \frac{\partial v}{\partial y} + \frac{\partial w}{\partial z} = 0 \quad (3)$$

$$\frac{\partial u}{\partial t} + \frac{\partial(uu)}{\partial x} + \frac{\partial(vu)}{\partial y} + \frac{\partial(wu)}{\partial z} = -g \frac{\partial z_s}{\partial x} + \frac{1}{\rho} \frac{\partial \tau_{xx}}{\partial x} + \frac{1}{\rho} \frac{\partial \tau_{xy}}{\partial y} + \frac{1}{\rho} \frac{\partial \tau_{xz}}{\partial z} + fv \quad (4)$$

$$\frac{\partial v}{\partial t} + \frac{\partial(uv)}{\partial x} + \frac{\partial(vv)}{\partial y} + \frac{\partial(wv)}{\partial z} = -g \frac{\partial z_s}{\partial y} + \frac{1}{\rho} \frac{\partial \tau_{yx}}{\partial x} + \frac{1}{\rho} \frac{\partial \tau_{yy}}{\partial y} + \frac{1}{\rho} \frac{\partial \tau_{yz}}{\partial z} - fu \quad (5)$$

The hydrostatic pressure assumption brings significant simplification to the full three-dimensional problem of Equations (1) and (2). However, this assumption is valid only for the gradually varying surface water flows. A full 3-D model without hydrostatic pressure assumption should be used in the regions of rapidly varying flows, such as flows around bridge piers, dikes, and bendway weirs (Wu et al., 2000a; Jia et al., 2001). Since most flows in rivers, estuaries and coastal zones can be assumed as shallow water flows, the hydrostatic pressure assumption has been often adopted. The 3-D models developed by Sheng (1983), Wang and Adefe (1986), Casulli and Cheng (1992), Jankowski et al. (1994), and Wu and Lin (2011) are based on the hydrostatic pressure assumption. At the free surface, the flow satisfies the kinematic condition given by Equation (6), where u_h , v_h , and w_h are the flow velocity components at the water surface.

$$\frac{\partial z_s}{\partial t} + u_h \frac{\partial z_s}{\partial x} + v_h \frac{\partial z_s}{\partial y} = w_h \quad (6)$$

Since low sediment concentration is assumed, the interactions among different size classes of moving sediment are ignored, and thus the transport of each size class of sediment can be handled individually. As shown in Figure 1, the moving sediment (total load or bed-material load) is divided into suspended load and bed load, and hence the flow depth h is divided into a bed-load layer with a thickness δ and the suspended-load layer above it with a thickness $h - \delta$. The exchange of sediment between the two layers is through deposition

(downward sediment flux) at a rate of D_{bk} and entrainment from the bed-load layer (upward flux) at a rate of E_{bk} .

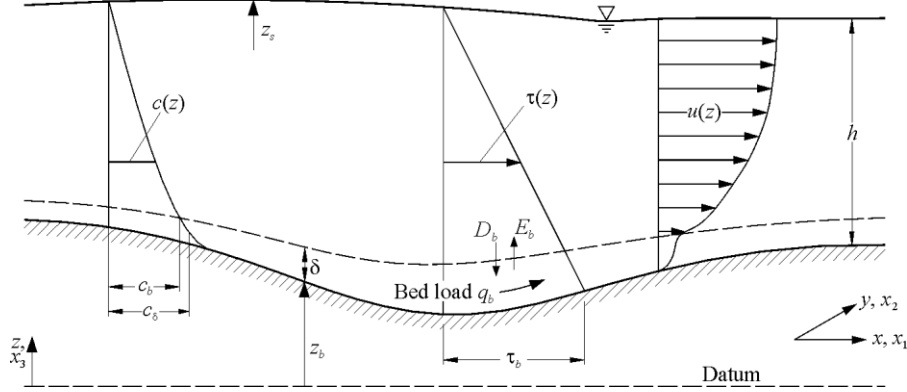


Figure 1. Configuration of flow and sediment transport (Wu et al., 2000a)

The distribution of sediment concentration in the suspended-load layer is governed by the convection-diffusion equation as given by Equation (7), where c_k is the local concentration of the k^{th} size class of suspended load, ω_{sk} is the sediment settling velocity, ε_s is the turbulent diffusivity coefficient of sediment. The turbulent diffusivity coefficient is determined as $\varepsilon_s = \nu_t / \sigma_c$, where σ_c is the turbulent Schmidt number, usually having a value between 0.5 and 1.0 or determined by using van Rijn's (1989) method. In Equation (7), δ_{j3} is the Kronecker delta with $j=3$ indicating the vertical direction, the subscript k denotes the sediment size class index, and N is the total number of sediment size classes. Note that the sediment size index k does not follow the summation convention in Equation (7) and the following equations.

$$\frac{\partial c_k}{\partial t} + \frac{\partial \left[(u_j - \omega_{sk} \delta_{j3}) c_k \right]}{\partial x_j} = \frac{\partial}{\partial x_j} \left(\varepsilon_s \frac{\partial c_k}{\partial x_j} \right) \quad (k=1, 2, \dots, N) \quad (7)$$

At the free surface, the vertical sediment flux is zero and hence the condition given by Equation (8) is applied. At the lower boundary of the suspended-load layer, the deposition rate is $D_{bk} = \omega_{sk} c_{bk}$, while the entrainment rate E_{bk} is given by Equation (9), where c_{b*k} is the capacity or equilibrium concentration at the reference level $z = z_b + \delta$ and needs to be determined using an empirical relation. Here, z_b is the bed surface elevation.

$$\left(\varepsilon_s \frac{\partial c_k}{\partial z} + \omega_{sk} c_k \right) \Big|_{z=z_s} = 0 \quad (8)$$

$$E_{bk} = -\varepsilon_s \frac{\partial c_k}{\partial z} \Big|_{z=z_b+\delta} = \omega_{sk} c_{b*k} \quad (9)$$

Depth-averaged Flow and Sediment Transport Equations

The depth-averaged quantity Φ of a three-dimensional variable φ is defined by Equation (10). Integrating Equations (3), (4), and (5) over the flow depth and using the Leibniz integral rule yields Equations (11), (12), and (13), respectively. In these equations, U and V are the depth-averaged flow velocities in x and y directions, T_{xx} , T_{xy} , T_{yx} , and T_{yy} are the depth-averaged turbulent stresses, D_{xx} , D_{xy} , D_{yx} , and D_{yy} are the dispersion terms due to the non-uniformity of flow velocity and the effect of secondary flow, which are important in the situations of curved channels. The bed shear stresses τ_{bx} and τ_{by} are determined by $\rho c_f U \sqrt{U^2 + V^2}$ and $\rho c_f V \sqrt{U^2 + V^2}$, respectively, where $c_f = gn^2/h^{1/3}$ and n is the Manning roughness coefficient. The stresses τ_{xx} and τ_{yy} represent the shear forces acting on the water surface, usually caused by winds.

$$\Phi = \frac{1}{h} \int_{z_b}^{z_s} \varphi dz \quad (10)$$

$$\frac{\partial h}{\partial t} + \frac{\partial(hU)}{\partial x} + \frac{\partial(hV)}{\partial y} = 0 \quad (11)$$

$$\begin{aligned} \frac{\partial(hU)}{\partial t} + \frac{\partial(hUU)}{\partial x} + \frac{\partial(hVU)}{\partial y} = & -gh \frac{\partial z_s}{\partial x} + \frac{1}{\rho} \frac{\partial(hT_{xx})}{\partial x} + \frac{1}{\rho} \frac{\partial(hT_{xy})}{\partial y} \\ & + \frac{\partial D_{xx}}{\partial x} + \frac{\partial D_{xy}}{\partial y} + \frac{1}{\rho} (\tau_{xx} - \tau_{bx}) + fhV \end{aligned} \quad (12)$$

$$\begin{aligned} \frac{\partial(hV)}{\partial t} + \frac{\partial(hUV)}{\partial x} + \frac{\partial(hVV)}{\partial y} = & -gh \frac{\partial z_s}{\partial y} + \frac{1}{\rho} \frac{\partial(hT_{yx})}{\partial x} + \frac{1}{\rho} \frac{\partial(hT_{yy})}{\partial y} \\ & + \frac{\partial D_{yx}}{\partial x} + \frac{\partial D_{yy}}{\partial y} + \frac{1}{\rho} (\tau_{yy} - \tau_{by}) - fhU \end{aligned} \quad (13)$$

Unlike the depth-averaged quantities defined by Equation (10), the depth-averaged suspended-load concentration, C_k , is defined by Equation (14), where U_s is the stream-wise depth-averaged velocity, and u_s is the local flow velocity projected to the stream-wise direction. By definition, $U_s = \left(\int_{z_b+\delta}^{z_s} u_s dz \right) / (h - \delta)$, but U_s is approximately set as the resultant depth-averaged velocity $\bar{U} = \sqrt{U^2 + V^2}$ at each vertical line.

$$C_k = \frac{1}{(h - \delta)U_s} \int_{z_b+\delta}^{z_s} u_s c_k dz \quad (14)$$

Integrating Equation (7), the three-dimensional sediment transport equation, over the suspended-load zone leads to Equation (15) as shown by Wu (2007), where S_{xk} and S_{yk} are the dispersion terms to account for the effect of the non-uniform distributions of flow velocity and sediment concentration. In nearly straight (or slightly curved) channels with simple geometry, the dispersion terms are usually combined with either the convection terms by introducing a correction factor or the diffusion terms by adjusting the diffusivity coefficient (then called the mixing coefficient). In curved channels, the dispersion terms become more important and will be discussed later. The parameter β_{sk} is a correction factor for suspended load, which is actually the ratio of the depth-averaged sediment and flow velocities. It

accounts for the temporal lag between flow and suspended-load transport in the depth-averaged 2-D model and is given by Equation (16).

$$\frac{\partial}{\partial t} \left(\frac{hC_k}{\beta_{sk}} \right) + \frac{\partial(UhC_k)}{\partial x} + \frac{\partial(VhC_k)}{\partial y} = \frac{\partial}{\partial x} \left(\varepsilon_s h \frac{\partial C_k}{\partial x} \right) + \frac{\partial}{\partial y} \left(\varepsilon_s h \frac{\partial C_k}{\partial y} \right) + \frac{\partial S_{sk}}{\partial x} + \frac{\partial S_{yk}}{\partial y} + E_{bk} - D_{bk} \quad (15)$$

$$\beta_{sk} = \left(\int_{z_b+\delta}^{z_s} u_s c_k dz \right) / \left(U_s \int_{z_b+\delta}^{z_s} c_k dz \right) \quad (16)$$

Integrating Equation (7) over the bed-load zone leads to the bed-load mass balance equation given by Equation (17), where p'_m is the porosity of bed material at the bed surface, q_{bk} is the bed-load transport rate by volume per unit time and width (m^2/s), u_{bk} is the bed-load velocity, and α_{bx} , α_{by} are the direction cosines of bed-load movement. The bed load is usually assumed to move along the direction of bed shear stress but may be affected by secondary flows in curved channels and gravity in channels with steep bed and bank slopes.

$$(1 - p'_m) \left(\frac{\partial z_b}{\partial t} \right)_k + \frac{\partial}{\partial t} \left(\frac{q_{bk}}{u_{bk}} \right) + \frac{\partial(\alpha_{bx} q_{bk})}{\partial x} + \frac{\partial(\alpha_{by} q_{bk})}{\partial y} = D_{bk} - E_{bk} \quad (17)$$

The first term on the left-hand side of Equation (17) represents the bed change, which results from the exchange between moving sediment and bed material. The second term accounts for the storage effect. Since the bed-load velocity u_{bk} is usually slower than the flow velocity, Equation (17) accounts for the temporal lag between flow and bed-load transport.

Summing Equations (15) and (17) leads to the bed-material load or total load transport equation given by Equation (18), where C_{tk} is the depth-averaged concentration of bed-material load, r_s is the ratio of suspended load to bed-material load, and β_{tk} is a correction factor for bed-material load related to β_{sk} and u_{bk} as shown in Equation (19).

$$(1 - p'_m) \left(\frac{\partial z_b}{\partial t} \right)_k + \frac{\partial}{\partial t} \left(\frac{hC_{tk}}{\beta_{tk}} \right) + \frac{\partial(UhC_{tk})}{\partial x} + \frac{\partial(VhC_{tk})}{\partial y} = \frac{\partial}{\partial x} \left[\varepsilon_s h \frac{\partial(r_s C_{tk})}{\partial x} \right] + \frac{\partial}{\partial y} \left[\varepsilon_s h \frac{\partial(r_s C_{tk})}{\partial y} \right] + \frac{\partial S_{sk}}{\partial x} + \frac{\partial S_{yk}}{\partial y} \quad (18)$$

$$\beta_{tk} = \frac{hC_{tk}}{hC_k / \beta_{sk} + q_{bk} / u_{bk}} \quad (19)$$

Near-Bed Sediment Exchange and Bed Change Equations

In the 3-D model, the suspended-load transport equation, Equation (7), is solved with the lower boundary condition specifying the deposition flux D_{bk} ($= \omega_{sk} c_{bk}$) and entrainment flux E_{bk} ($= \omega_{sk} c_{b^*k}$). The problem is closed by using an empirical formula to determine the near-bed suspended-load capacity concentration c_{b^*k} . However, in the depth-averaged 2-D (or 1-D) model, the deposition flux D_{bk} is usually determined by relating the near-bed suspended-

load concentration c_{bk} to the depth-averaged suspended concentration C_k , because c_{bk} is not a dependent variable to be solved. The entrainment flux E_{bk} can be determined by using an empirical formula for c_{b^*k} or by relating c_{b^*k} to the depth-averaged suspended-load capacity concentration C_{*k} that is determined using an empirical formula. Therefore, the net exchange flux can be determined using Equation (20) as proposed by Han (1980), where α is the adaptation coefficient of suspended load.

$$D_{bk} - E_{bk} = \alpha \omega_{sk} (C_k - C_{*k}) \quad (20)$$

In the case of only suspended-load transport, Equation (20) is often used to determine the bed change as described by Equation (21). In the case of only bed-load transport, Daubert and Lebreton (1967), Wellington (1978), Nakagawa and Tsujimoto (1980), Phillips and Sutherland (1989), and Thuc (1991) used the relationship given by Equation (22), where L_b is the adaptation length of bed load and q_{b^*k} is the equilibrium or capacity transport rate of bed load.

$$(1 - p'_m) \left(\frac{\partial z_b}{\partial t} \right)_k = D_{bk} - E_{bk} \quad (21)$$

$$(1 - p'_m) \left(\frac{\partial z_b}{\partial t} \right)_k = \frac{1}{L_b} (q_{bk} - q_{b^*k}) \quad (22)$$

For general cases, in which bed load and suspended load are equivalently important, Equation (23) is used for bed change (Wu, 2007), where L is the adaptation length of sediment. Note that even though Equation (23) seems to be the summation of Equations (21) and (22), L is not the same as the bed-load adaption length L_b , due to the interaction between bed load, suspended load and bed material. This will be explained later in more detail. Equation (23) assumes that the exchange between suspended load and bed load directly contributes to bed changes. As bed load is located between suspended load and bed material, the exchange between suspended load and bed load results in change of bed load first and in turn bed surface change. However, the bed load layer is usually very thin, so that the assumption in Equation (23) is acceptable. Substituting Equation (23) into Equation (17) yields Equation (24) for the non-equilibrium transport of bed load.

$$(1 - p'_m) \left(\frac{\partial z_b}{\partial t} \right)_k = D_{bk} - E_{bk} + \frac{1}{L} (q_{bk} - q_{b^*k}) \quad (23)$$

$$\frac{\partial}{\partial t} \left(\frac{q_{bk}}{u_{bk}} \right) + \frac{\partial (\alpha_{bx} q_{bk})}{\partial x} + \frac{\partial (\alpha_{by} q_{bk})}{\partial y} = \frac{1}{L} (q_{b^*k} - q_{bk}) \quad (24)$$

Thus, bed load is determined with Equation (24) and suspended load is determined with Equations (7) and (15) in the 3-D and depth-averaged 2-D models, respectively. The bed change can be determined with Equation (23) or the overall sediment balance equation that is derived by summing Equation (17) with Equation (15) or Equation (7) integrated over the suspended-load zone. This approach is based on separation of suspended load and bed load. The important parameters include the sediment adaptation length L , the bed-load transport capacity q_{b^*k} , and the suspended-load near-bed capacity concentration c_{b^*k} in a 3-D model. In a depth-averaged 2-D model, the important parameters are L , q_{b^*k} , the suspended-load

depth-averaged capacity concentration C_{*k} , and the suspended-load adaptation coefficient α . The sediment transport capacity quantities need to be determined using empirical formulas, which can be written in a general form as given by Equation (25), where p_{bk} is the bed material gradation at the mixing (surface) layer; c_{bk}^* and C_k^* are the potential near-bed and depth-averaged capacity concentrations of the k^{th} size class of suspended load, respectively, and q_{bk}^* is the potential capacity transport rate of the k^{th} size class of bed load.

$$q_{b^{*k}} = p_{bk} q_{bk}^*, \quad c_{b^{*k}} = p_{bk} c_{bk}^*, \quad \text{or} \quad C_{*k} = p_{bk} C_k^* \quad (k=1,2,\dots,N) \quad (25)$$

An alternative NEST modelling approach in the depth-averaged 2-D (or 1-D) model is to combine bed load and suspended load as bed-material load, whose mass balance is governed by Equation (18). To close this approach, the near-bed exchange flux relation given by Equation (26) is used, where α_t and L_t are the adaptation coefficient and length of bed-material load (or total load), respectively, q_{tk} and $q_{t^{*k}}$ are the actual and capacity transport rates of bed-material load (or total load), respectively, and $C_{t^{*k}}$ is the bed-material load capacity concentration. The adaptation coefficient, α_t , is related to L_t by $\alpha_t = L_t \omega_s / (\bar{U}h)$. Substituting Equation (26) into Equation (18) leads to the bed-material load transport equation given by Equation (27).

$$(1 - p'_m) \left(\frac{\partial z_b}{\partial t} \right)_k = \alpha_t \omega_{sk} (C_{tk} - C_{t^{*k}}) = \frac{q_{tk} - q_{t^{*k}}}{L_t} \quad (26)$$

$$\begin{aligned} \frac{\partial}{\partial t} \left(\frac{hC_{tk}}{\beta_{tk}} \right) + \frac{\partial(UhC_{tk})}{\partial x} + \frac{\partial(VhC_{tk})}{\partial y} = \frac{\partial}{\partial x} \left[\varepsilon_s h \frac{\partial(r_s C_{tk})}{\partial x} \right] + \frac{\partial}{\partial y} \left[\varepsilon_s h \frac{\partial(r_s C_{tk})}{\partial y} \right] \\ + \frac{\partial S_{xk}}{\partial x} + \frac{\partial S_{yk}}{\partial y} + \alpha_t \omega_{sk} (C_{t^{*k}} - C_{tk}) \end{aligned} \quad (27)$$

Consequently, the bed-material load is determined with Equation (27), and the bed change is determined using Equation (26). This approach solves one less transport equation than the suspended-load and bed-load separation approach for each sediment size class. This is computationally more efficient when multiple sediment size classes are considered. The important parameters in this approach are the adaptation coefficient α_t (or adaptation length L_t) and the bed-material load transport capacity. The latter is determined using an empirical formula given by Equation (28), where C_{tk}^* is the potential capacity concentration of the k^{th} size class of bed-material load.

$$C_{t^{*k}} = p_{bk} C_{tk}^* \quad (k=1,2,\dots,N) \quad (28)$$

Note that the governing equations for only the 2-D and 3-D models are described above. The depth-averaged 2-D model equations can be reduced to 1-D equations by eliminating the terms for lateral direction. More generally, one can derive the 1-D model equations by integrating Equations (3)–(5) and (7) over the cross-section. The details can be found in Wu (2007).

Bed Material Sorting Equation

To account for the variation of bed material gradation in time and space, the bed material is often divided into several layers at each computational node. The surface layer is the mixing layer that directly participates in the exchange with the sediment moving with the flow. Based on mass balance, Equation (29) for the variation of bed material gradation in the mixing layer can be derived (Wu, 1991; Wu et al., 2004), where p_{bk} is the bed material gradation in the mixing layer, δ_m is the mixing layer thickness, which is related to bed material size or bed form height. In the above equation, the bed deformation rate, $\partial z_b / \partial t$, is given by $\partial z_b / \partial t = \sum_{k=1}^N (\partial z_b / \partial t)_k$, p_{bk}^* is p_{bk} when $\partial \delta_m / \partial t - \partial z_b / \partial t \leq 0$, and p_{bk}^* is the bed material gradation at the subsurface layer (below the mixing layer) when $\partial \delta_m / \partial t - \partial z_b / \partial t > 0$. The last term on the right-hand side represents the exchange between the mixing layer and the subsurface layer.

$$\frac{\partial(\delta_m p_{bk})}{\partial t} = \left(\frac{\partial z_b}{\partial t} \right)_k + p_{bk}^* \left(\frac{\partial \delta_m}{\partial t} - \frac{\partial z_b}{\partial t} \right) \quad (29)$$

The bed material sorting model in Equation (29) is similar to Karim and Kennedy's (1982) mixing layer model, but different from Spasojevic and Holly's (1993) active layer model, where the active layer includes the bed-load layer and the mixing layer.

AUXILIARY RELATIONS

Turbulence Closure

The turbulent stresses in the 2-D and 3-D models need to be determined by turbulence closure models. Most of the common turbulence models are based on Boussinesq's eddy viscosity concept shown in Equation (30), where k is the turbulent kinetic energy, and ν_t is the turbulent or eddy viscosity. The eddy viscosity is usually determined by the parabolic model, the mixing length model, or the linear $k - \varepsilon$ turbulence models. The linear $k - \varepsilon$ turbulence models include the standard, low-Reynolds number, RNG, and non-equilibrium $k - \varepsilon$ turbulence models.

$$\tau_{ij} = \rho \nu_t \left(\frac{\partial u_i}{\partial x_j} + \frac{\partial u_j}{\partial x_i} \right) - \frac{2}{3} k \delta_{ij} \quad (30)$$

The Boussinesq's assumption, which adopts an isotropic eddy viscosity for all Reynolds stresses, fails for the flows with sudden changes in mean-strain rate or with "extra" rates of strain, e.g. curvilinear flows. In these cases, the Reynolds stresses adjust to such changes at a rate unrelated to the mean flow processes and time scale. To capture this kind of turbulence-generated flow features, the non-linear $k - \varepsilon$ turbulence model, the Reynolds-stress/flux model and the algebraic stress/flux model should be used (Rodi, 1993). In addition, Large Eddy Simulation (LES) and Direct Numerical Simulation (DNS) have also been used in modeling of sediment-laden flows.

Channel Roughness

In natural rivers, the banks and bed usually have different roughness. The bank roughness elements include bank materials, channel training works, hydraulic structures, and vegetation, while the bed roughness elements include rigid materials as well as movable bed forms, such as ripples, dunes, alternate bars, and islands. For the banks and rigid bed, a constant roughness can be used. For the movable bed in an alluvial river, the bed roughness changes with flow conditions and is thus more difficult to evaluate. Einstein and Barbarossa (1952), Engelund and Hansen (1967), van Rijn (1984c), Wu and Wang (1999) and others have proposed empirical or semi-empirical methods to calculate the roughness on movable beds. However, because these empirical relations usually rely on the data sets used and may give different predictions at different sites or times; caution must be exercised when applying them to a site-specific study. The most reliable approach to handle the channel roughness is still calibration using the available data measured at the study site.

Sediment Adaptation Length and Coefficient

The adaptation length, which characterizes the distance for sediment to adjust from a non-equilibrium state to the equilibrium state, is a very important parameter in the NEST model. Traditionally, the adaptation length of suspended load is given by Equation (31). The coefficient α can be calculated with Armanini and di Silvio's (1988) method, Zhou and Lin's (1998) method, or other semi-empirical methods, which were developed with simplifications and assumptions, usually for flat beds. Values of α calculated from these methods are usually larger than 1. However, in practice, α has been given different values by many researchers, most of them being less than 1. Based on results obtained from validation tests of 1-D models in many reservoirs and rivers, it has been suggested that a value of 1 should be used for the case of strong erosion, 0.25 for strong deposition, and 0.5 for weak erosion and deposition (Han, 1980; Wu, 1991; Wu et al., 2004).

$$L_s = \frac{\bar{U}h}{\alpha\omega_s} \quad (31)$$

For bed load, Bell and Sutherland (1983) found that the adaptation length L_b is a function of time t in an experimental case of bed degradation downstream of a dam due to clear water inflow. In numerical modeling, Nakagawa and Tsujimoto (1980), Phillips and Sutherland (1989), Thuc (1991), and Wu et al. (2000a) adopted L_b as the average saltation step length of sand on the bed as observed in laboratory experiments, while Rahuel et al. (1989) and Fang (2003) used much larger values for L_b (one to two times the numerical grid length) in the case of natural rivers. One reason for the disparity is that the adaptation length, especially for bed load, is closely related to the dimensions of the sediment movements, bed forms, and channel geometry of each study case, which are significantly different between laboratory and field situations. In laboratory experiments, sediment transport processes are of small scales, such as sand saltation, ripples, and dunes, while in streams sediment transport processes occur usually at larger scales in longer periods. More recently, Wu et al. (2004) suggested that the adaptation length of bed load may be the same as the dimension of the dominant bed forms, such as the length of sand dunes (about 5–10 times the flow depth) in laboratory flume cases, and the length of alternate bars (about 6.3 times the channel width,

Yalin 1972) in field cases. This suggestion has given very promising results in a series of applications.

Because bed-material load is a combination of bed load and suspended load, its adaptation length L_t can be given the larger of L_b and L_s values (Wu et al., 2004) as described by Equation (32) or a weighted average of L_b and L_s as given by Equation (33).

$$L_t = \max\{L_b, L_s\} \quad (32)$$

$$L_t = (1 - r_s)L_b + r_s L_s \quad (33)$$

By comparing Equations (23) and (26), one can find that the adaptation length L in Equation (23) is approximately equal to L_t in Equation (26). This can be derived by assuming that the bed-load layer is very thin and in turn $\alpha_t \approx \alpha$. On the other hand, L or L_t reduces to L_b in the case of only bed-load transport.

It should be pointed out that the values of adaptation length and coefficient vary in different cases. Calibration using available measurement data is recommended to obtain more reliable results for real-life problems.

Bed-Load and Suspended-Load Velocities

Bed load usually moves by rolling, sliding, and saltation, depending on flow and sediment conditions. Saltation is the dominant mode of bed-load transport, while rolling (and to a lesser extent, sliding) occurs only near the threshold of entrainment and between individual saltation jumps (Bridge and Dominic, 1984). van Rijn (1984a) investigated the characteristics of particle saltation and developed an empirical formula for the bed-load velocity. Wu et al. (2006) verified van Rijn's formula using three sets of experimental data measured by Francis (1973), Luque and van Beek (1976) and Lee and Hsu (1994), and recalibrated the bed-load velocity formula as given by Equation (34), where γ_s and γ are the specific weights of sediment and water, respectively, d is the sediment diameter, T is the transport stage number defined as $T = \tau_b / \tau_c - 1$, with τ_b being the total bed shear stress measured in the three experiments where no significant bed forms developed. The coefficient and exponent in the original van Rijn's formula are 1.5 and 0.6, respectively.

$$\frac{u_b}{\sqrt{(\gamma_s / \gamma - 1)gd}} = 1.64T^{0.5} \quad (34)$$

There is a lag between the local flow and suspended-load velocities. This has been observed experimentally by Muste and Patel (1997) and discussed in detail by Cheng (2004). A two-phase flow model (Wu and Wang, 2000; Greimann and Holly, 2001) can be used to describe this local velocity lag in general situations. However, according to the experimental observations of Muste and Patel (1997), the local stream-wise velocity of suspended load with a diameter of 0.23 mm is less than the local flow velocity by as much as 4%. This local velocity difference is negligible in comparison with the depth-averaged flow and suspended-load velocity difference (Wu et al., 2006). Thus, the local velocity lag may be ignored, and only the depth-averaged velocity lag is discussed below.

Equation (16) can be rewritten as $\beta_s = U_{sed} / U$, in which U_{sed} is the concentration-weighted velocity of suspended load. Because higher sediment concentration corresponds to

smaller flow velocity near the channel bottom while lower sediment concentration corresponds to larger flow velocity in the upper flow layer, $U_{sed} \leq U$ and β_s normally is less than 1. By using the logarithmic distribution of flow velocity, $u = U \{1 + \sqrt{g} [1 + \ln(z/h)] / (C_h \kappa)\}$, and the Rouse distribution of suspended-load concentration with the reference level set at $0.01h$, Wu et al. (2006) obtained the relation of β_s with the Rouse number $\omega_s / (\kappa U_*)$ and the Chezy coefficient C_h , as shown in Figure 2. It can be seen that β_s decreases as the Rouse number increases and the Chezy coefficient decreases. For fine sediments, β_s is close to 1 and the lag between the depth-averaged flow and sediment velocities can be ignored. However, for coarse sediments, this lag can be up to 60% of the flow velocity and should be considered.

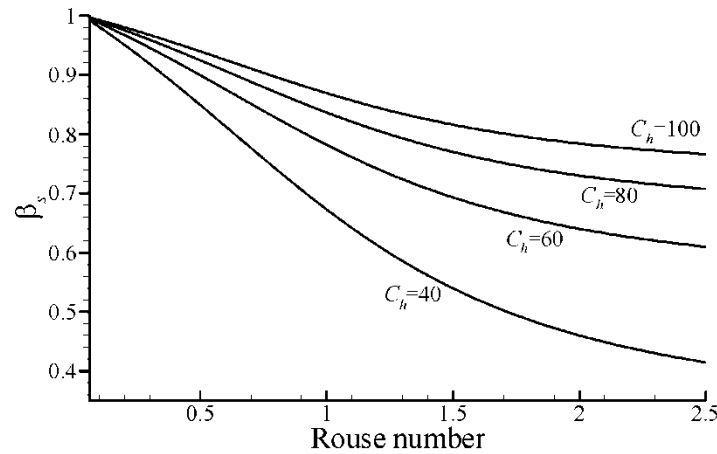


Figure 2. Factor β_s as a function of the Rouse number and the Chezy coefficient

Non-cohesive Sediment Transport Capacity

The sediment transport capacity formulas proposed by Meyer-Peter and Mueller (1948), Dou (1963), Yalin (1972), and van Rijn (1984a) are often used to calculate the discharge of uniform bed load. These formulas are also used for the total discharge of non-uniform bed load. For the fractional discharge of non-uniform bed load, the pioneering research was attributed to Einstein (1950), followed by Parker et al. (1982), Wu et al. (2000b), and others. One of the most widely recognized methods for the suspended-load discharge is the Einstein's (1950) method, which integrates the product of sediment concentration c and stream-wise flow velocity u over the suspended-load layer. However, the empirical formulas proposed by van Rijn (1984b) and Zhang (1961) (see Zhang and Xie, 1993) for the total discharge of suspended load are much simpler than Einstein's (1950) method and have comparable reliability. Wu et al. (2000b) established a formula to directly calculate the fractional discharge of non-uniform suspended load.

The total discharge of bed-material load can be determined by the methods proposed by Einstein (1950), Engelund and Hansen (1967), Ackers and White (1973), Yang (1973), and van Rijn (198a, b). For the fractional discharge of non-uniform bed-material load, the

modified Ackers and White's (1973) formula (Day, 1980; Proffit and Sutherland, 1983), SEDTRA module (Garbrecht et al., 1995), and Wu et al. (2000b) have been often used.

The capacity near-bed concentration of uniform suspended-load can be determined by using the methods proposed by van Rijn (1984b), Zyserman and Fredsøe (1994) and others. For the fractional near-bed concentration of non-uniform suspended load, the empirical formulas proposed by Einstein (1950) and Garcia and Parker (1991) can be used. However, two issues should be noted. One is that the measurement of suspended-load concentration near the channel bed is very difficult. Usually, the near-bed concentrations have to be extrapolated from the measured sediment concentrations in the upper zone with the aid of an assumed concentration profile along the water depth. Therefore, the accuracy and reliability of this analysis are highly dependent on the selection of sediment concentration distribution near the bed. The other important issue is that different reference levels have been used to define the near-bed concentration in different formulas.

The sediment transport capacity formulas in the literature are mostly empirical or semi-empirical and have large discrepancy among them. Comparisons of the total-discharge formulas have been performed by Brownlie (1981), Yang and Wan (1991), and others. Most of these tests show that Ackers and White's (1973), Engelund and Hansen's (1967), and Yang's (1973) formulas are relatively reliable for the total discharge of bed-material load. Ribberink et al. (2002) and Wu and Wang (2003) tested the formulas for the fractional discharge of non-uniform bed-material load, and found that the Wu et al. (2000b) formula and the SEDTRA module perform better. However, calibration and validation using site-specific data is highly recommended before applying a sediment transport formula to a real-life problem.

The formulas of Wu et al. (2000b) for fractional bed-load and suspended-load transport capacity are given by Equations (35) and (36), respectively, where q_{b^*k} and q_{s^*k} are the bed-load and suspended-load transport rates of sediment size class k by volume per unit time and width (m^2/s), d_k is the representative diameter of size class k of the sediment mixture, p_{bk} is the fraction of sediment size class k in the surface layer of bed material, $\tau_{cri,k}$ is the critical shear stress for the incipient motion of sediment size k on the bed, U is the depth-averaged flow velocity, τ is the shear stress on the wetted perimeter of the cross-section including bed and banks, and τ'_b is the bed shear stress corresponding to the grain roughness. The bed shear stress corresponding to the grain roughness is given by $\tau'_b = (n'/n)^{3/2} \tau_b$, where τ_b is the bed shear stress, n' is the Manning coefficient of grain roughness calculated with $n' = d_{50}^{1/6}/20$, and n is the Manning coefficient of bed roughness (including grain and form roughness).

$$\frac{q_{b^*k}}{p_{bk} \sqrt{(\gamma_s / \gamma - 1) g d_k^3}} = 0.0053 \left(\frac{\tau'_b}{\tau_{cri,k}} - 1 \right)^{2.2} \quad (35)$$

$$\frac{q_{s^*k}}{p_{bk} \sqrt{(\gamma_s / \gamma - 1) g d_k^3}} = 0.0000262 \left[\left(\frac{\tau}{\tau_{cri,k}} - 1 \right) \frac{U}{\omega_{sk}} \right]^{1.74} \quad (36)$$

Using the bed-load transport rate relation $q_{b^*k} = \delta c_{b^*k} u_{bk}$ and Equations (34) and (35) yields Equation (37) for near-bed suspended-load capacity concentration, where δ is the bed-

load layer thickness, set as $\max(2d_{50}, 0.01h, 0.5\Delta_r)$, in which d_{50} is the median diameter of bed material, h is the water depth, and Δ_r is the sand ripple height. The coefficient a is about 1.64 according to Equation (34) and can be set as a calibration parameter.

$$c_{b^*k} = 0.0053 p_{bk} \frac{d_k}{a\delta} \left(\frac{\tau'_b}{\tau_{cri,k}} - 1 \right)^{1.7} \quad (37)$$

Another issue related to non-uniform sediment transport capacity is that the hiding and exposure mechanism in bed material needs to be considered through the introduction of correction factors in the formulas. Coarse particles have higher chances of exposure to the flow, while fine particles are more likely sheltered by coarse particles. This hiding and exposure mechanism significantly affects non-uniform sediment transport. The correction factors of Egiazaroff (1965), Ashida and Michiue (1971), Hayashi et al. (1980), and Parker et al. (1982) are functions of the non-dimensional sediment size d_k/d_m or d_k/d_{50} . These functions are simple but do not consider the effect of bed material size composition. Wu et al. (2000b) derived the hiding and exposure probabilities of sediment particles in the bed using the bed material size composition and suggested Equation (38) for the critical shear stress for non-uniform sediment incipient motion, where Θ_{cri} is the critical Shield number for the incipient motion of the mean or median diameter of the bed sediment, and m is an empirical parameter. Using laboratory and field data, the calibrated values were found to be $\Theta_{cri} = 0.03$ and $m = 0.6$. The hidden (p_{hk}) and exposed (p_{ek}) probabilities of particles d_k in the bed material are given by Equation (39).

$$\frac{\tau_{cri,k}}{(\gamma_s - \gamma)d_k} = \Theta_{cri} \left(\frac{p_{ek}}{p_{hk}} \right)^{-m} \quad (38)$$

$$p_{hk} = \sum_{j=1}^N p_{bj} \frac{d_j}{d_k + d_j}, \quad p_{ek} = \sum_{j=1}^N p_{bj} \frac{d_k}{d_k + d_j} \quad (39)$$

The critical shear stress $\tau_{cri,k}$ determined with Equation (38) is used in the fractional bed-load and suspended-load transport capacity formulas of Wu et al. (2000b), Equations (35) and (36), to consider the effect of hiding and exposure mechanism on sediment transport.

Sediment Transport on Steep Slope

For a steep bed or bank slope, the effect of the gravity on sediment transport is an important factor. Two approaches have been applied in literature to consider this effect in the sediment transport capacity formula that can be written as $q_{b^*} = f(\tau_b/\tau_c)$, where τ_b is the bed shear stress and τ_c is the critical shear stress for the incipient motion of bed material. One approach is to correct the critical shear stress τ_c using the method of Brooks (1963) or van Rijn (1989). The other approach is to add the stream-wise component of the gravitational force in the bed shear τ_b , as shown in Equation (40), without modifying τ_c (Wu, 2004), where τ_{be} is the effective tractive force, ϕ is the bed angle with the horizontal, with positive values denoting downslope bed, ϕ is the repose angle, and λ_0 is a coefficient related to flow

and sediment conditions as well as the bed slope (Wu, 2004). Equation (40) can be used to modify many sediment transport formulas, such as the van Rijn (1984a, b) formula and the Wu et al. (2000b) formula.

$$\tau_{be} = \tau_b + \lambda_0 \tau_c \sin \phi / \sin \varphi \quad (40)$$

The effect of the gravity on the direction of bed-load transport has been investigated by Engelund (1974), Sekine and Parker (1992), and Wu (2004). To account for gravity, the parameters α_{bx} and α_{by} in Equation (24) are replaced by $\alpha_{bx,e}$ and $\alpha_{by,e}$ as shown in Equation (41), where ϕ_x and ϕ_y are the bed angles in the x and y directions (Wu, 2004).

$$\left. \begin{aligned} \alpha_{bx,e} &= \alpha_{bx} \tau_b + \lambda_0 \tau_c \sin \phi_x / \sin \varphi \\ \alpha_{by,e} &= \alpha_{by} \tau_b + \lambda_0 \tau_c \sin \phi_y / \sin \varphi \end{aligned} \right\} \quad (41)$$

Effect of Helical Flow in Curved Channel

Helical (secondary) motions in curved channels play an important role in the evolution of channel morphology, inducing deposition along the inner bank and erosion along the outer bank. This phenomenon can be simulated with a three-dimensional model, as shown by Wu et al. (2000a) and others. However, to reduce computation time, a number of investigators, e.g., Flokstra (1977), Jin and Steffler (1993), and Wu and Wang (2004) have modified the depth-averaged 2-D models to include the effect of the secondary helical motions. The dispersion terms in Equations (12), (13) and (15) can be used to serve this purpose. Jin and Steffler (1993) calculated these terms by solving two extra equations that are obtained by integrating the 3-D horizontal moment-of-momentum equations over the depth. Flokstra (1977) and Wu and Wang (2004) determined these terms by using Equation (42) for the vertical distribution of the helical flow and the Rouse distribution or Lane-Kalinske distribution for the suspended-load concentration along the depth.

$$u_n = U_n + b_s I \left(\frac{2z}{h} - 1 \right) \quad (42)$$

In Equation (42), u_n is the local velocity in the cross-stream direction, U_n is the depth-averaged velocity in the cross-stream direction, b_s is the coefficient with a value of about 6.0, and I is the intensity of helical flow. Theoretically, $I = U_s h / r$ at the channel centerline (Rozovskii, 1957). Here, r is the local radius of curvature. For the entire channel bend, de Vriend (1981) proposed a differential transport equation to determine I . Wu and Wang (2004) simplified this differential equation into Equation (43) for the helical flow intensity in the fully developed region, where β_l is an empirical coefficient, B is the channel width at the water surface, η is the dimensionless transverse coordinate (y' / B), with $\eta = 0$ at the inner bank and $\eta = 1$ at the outer bank, and $T_a D_l = \lambda_l r_c n \sqrt{g} h^{5/6}$ with λ_l being an empirical coefficient and r_c the radius of curvature at the channel centerline.

$$\frac{rI}{\beta_l h U_s} = 1 - \frac{1 - e^{-B/\sqrt{T_a D_l}}}{e^{B/\sqrt{T_a D_l}} - e^{-B/\sqrt{T_a D_l}}} e^{B\eta/\sqrt{T_a D_l}} - \frac{e^{B/\sqrt{T_a D_l}} - 1}{e^{B/\sqrt{T_a D_l}} - e^{-B/\sqrt{T_a D_l}}} e^{-B\eta/\sqrt{T_a D_l}} \quad (43)$$

Equation (43) shows that the helical flow intensity profile along the cross-section is determined by β_l and λ_l . Usually, β_l determines the magnitude of I , while λ_l determines its lateral distribution. According to calibrations using laboratory and field measurements, β_l is in the range of 1.0–2.0, and λ_l has a value of about 3.0.

By using the power law for the stream-wise flow velocity and the linear model, Equation (43), for the helical flow velocity, Wu and Wang (2004) derived dispersion transports in Equations (12) and (13) as shown in Equations (44), (45), and (46). In these equations, α_{ii} are the coefficients of transformation between the (x, y) and (s, n) coordinate systems and m is usually about 7.

$$D_{xx} = -h \left[\frac{1}{m(m+2)} \alpha_{11} \alpha_{11} U_s^2 + \frac{2b_s}{2m+1} \alpha_{11} \alpha_{12} I U_s + \frac{b_s^2}{3} \alpha_{12} \alpha_{12} I^2 \right] \quad (44)$$

$$D_{xy} = -h \left[\frac{1}{m(m+2)} \alpha_{11} \alpha_{21} U_s^2 + \frac{b_s}{2m+1} (\alpha_{11} \alpha_{22} + \alpha_{12} \alpha_{21}) I U_s + \frac{b_s^2}{3} \alpha_{12} \alpha_{22} I^2 \right] \quad (45)$$

$$D_{yy} = -h \left[\frac{1}{m(m+2)} \alpha_{21} \alpha_{21} U_s^2 + \frac{2b_s}{2m+1} \alpha_{21} \alpha_{22} I U_s + \frac{b_s^2}{3} \alpha_{22} \alpha_{22} I^2 \right] \quad (46)$$

By using the power law for the stream-wise flow velocity, the linear law for the helical flow velocity and the Lane-Kalinske distribution for the suspended-load concentration, Wu and Wang (2004) derived the suspended-load dispersion fluxes in Equation (15) as given by Equations (47) and (48). The function $f(z)$ is given by Equation (49) and Π is defined by Equation (50). In addition, for the effect of the helical flow on the bed-load transport direction, the methods proposed by Engelund (1974) and Odgaard (1981) can be used.

$$S_{xk} \approx -\alpha_{12} b_s I C_k \int_{\delta}^h \left(2 \frac{z}{h} - 1 \right) f(z) dz \quad (47)$$

$$S_{yk} \approx -\alpha_{22} b_s I C_k \int_{\delta}^h \left(2 \frac{z}{h} - 1 \right) f(z) dz \quad (48)$$

$$f(z) = \frac{m}{m+1} \Pi^{-1} \exp \left(-\frac{15 \omega_{sk} z}{U_* h} \right) \quad (49)$$

$$\Pi = \int_{\delta/h}^1 \zeta^{1/m} e^{-15 \omega_{sk} \zeta / U_*} d\zeta \quad (50)$$

Local Scour near In-stream Structures

The local scour near in-stream structures, such as bridge piers, abutments and spur-dykes, is significantly affected by the three-dimensional local flow features, such as the downward flow, horseshoe and wake vortices, the localized pressure gradient, and turbulence intensity. At present, the highly complex, three-dimensional near-field flows can be calculated reasonably well with advanced turbulence models, such as linear and non-linear $k-\varepsilon$ turbulence models and LES. The suspended-load and bed-load transport near in-stream structures can be calculated using Equations (7) and (24), respectively. However, it has been found that some model parameters, such as sediment transport capacity and adaptation length,

may be different for gradually and rapidly varied flows. In particular, the sediment transport capacity of rapidly varied flows is affected by the aforementioned local flow features. Based on the analysis of the forces acting on sediment particles near the bed exerted by rapidly-varied flows, Wu (2007) modified the van Rijn (1984a, b) formulas of equilibrium bed-load transport rate and near-bed suspended-load concentration for the simulation of local scour by determining the effective tractive stress, τ_e , and critical shear stress for sediment incipient motion, τ_c , as given by Equation (51).

$$\left. \begin{aligned} \tau_e &= \tau'_b - \frac{a\pi}{6} d (\nabla p_d)_s \\ \tau_c &= K_p K_d K_g \tau_{c0} \end{aligned} \right\} \quad (51)$$

In Equation (51), p_d is the dynamic (non-hydrostatic) pressure, $(\nabla p_d)_s$ is the stream-wise gradient of dynamic pressure near the bed, d is the sediment size, a is a coefficient assumed as $4/\pi$, τ_{c0} is the critical shear stress for sediment incipient motion on a flat bed under uniform flow determined using the Shields curve, and K_p , K_d , K_g are the correction factors due to the effects of vertical dynamic pressure gradient, downward flow, and bed slope. The correction factors are defined in Equation (52), where β is the impact angle of flow to the bed.

$$\left. \begin{aligned} K_p &= 1 + \frac{1}{(\rho_s - \rho)g} \frac{\partial p_d}{\partial z} \\ K_d &= \frac{1}{1 + \sin \beta} \\ K_g &= \frac{\sin(\varphi - \phi)}{\sin \varphi} \end{aligned} \right\} \quad (52)$$

An alternative approach can be derived by removing the correction factor K_g from the second relation in Equation (51), but adding the stream-wise gravity component in the effective tractive stress in the first relation as shown in Equation (40).

Bank Erosion and Mass Failure

Bank erosion is the main cause of channel widening and meandering. To realistically model the morphological evolution of channels with movable banks, both bed and bank changes should be simulated (Duan et al., 2001; Wu et al., 2004). Usually, for a non-cohesive bank, the bank material fails in particles when the slope angle is larger than the repose angle. The particles slide to the bank toe and form a new slope with the repose angle. In the simulation of this sliding (avalanche) process, mass conservation should be satisfied. Wu (2007) presented such an algorithm, which considers a cluster comprising of a cell centered by node P with its eight adjacent cells based on a rectangular or quadrilateral mesh. The slope angle between node P and each of the eight adjacent nodes is checked against the repose angle and the mass balance equation is derived and used to calculate the sliding flux and in turn the bed change on the cluster. This algorithm was later improved by adopting different repose angles for the submerged sediment and the emergent sediment above the water surface

(Wu et al., 2012). The emergent sediment above the water surface may exhibit apparent cohesion due to suction and moisture and thus have steeper repose angle than the submerged sediment.

For a cohesive bank, the bank material collapses in the form of mass failure, a discontinuous phenomenon. The bank instability and mass failures may be caused by bed degradation and lateral fluvial erosion at bank toes as well as the pore pressure change in the bank soil. Bank failures can be planar, rotational, cantilever, or piping- or sapping-type. Planar and rotational failures usually occur on the homogeneous, non-layered banks, whereas cantilever failures usually happen on the layered banks. Piping- or sapping-type failures most likely occur on the heterogeneous banks where seepage flow is often observed.

Arulanandan et al. (1980) established an empirical relationship for calculating the erosion of bank toes. Osman and Thorne (1988) proposed an algorithm to analyze the stability of cohesive banks, with the safety factor being defined as the ratio of the resistance and driving forces for the failure. Simon et al. (2000) proposed a more sophisticated bank stability and toe erosion model, which considers wedge-shaped bank failures with several distinct bank material layers and user defined bank geometry. This model is able to incorporate root reinforcement and surcharge effects of six vegetation species, including willows, grasses and large trees, and simulate saturated and unsaturated soil strength considering the effect of pore-water pressure.

NUMERICAL METHODS

Discretization of Governing Equations

The flow and sediment transport equations are of the convection-diffusion type. The numerical methods often used to discretize these equations include finite difference method, finite volume method, finite element method, and finite analytical method. The diffusion terms are usually discretized with the central difference scheme. However, the convection terms have to be discretized with an upwind scheme. The simplest one is the first-order upwind scheme, which is very stable but has strong numerical diffusion. The often adopted numerical techniques with upwind schemes and acceptable numerical diffusion include the hybrid upwind/central difference scheme, exponential difference scheme (Spalding, 1972), finite analytical scheme, HLP (hybrid linear/parabolic approximation) scheme (Zhu, 1991), and upwind interpolation scheme (Wang and Hu, 1992). This group of schemes usually has second-order accuracy or less. Some high-order upwind schemes, such as QUICK scheme (Leonard, 1979), have higher than second-order accuracy, but may encounter numerical oscillations. Limiters have been developed to control the potential numerical oscillations caused by these high-order upwind schemes.

For unsteady problems, the time derivative terms can be discretized by using either an explicit or an implicit scheme. The explicit scheme results in simple algebraic equations and computer program and can be easily parallelized. However, the time step in the explicit scheme is usually limited by the CFL condition. The implicit scheme allows a larger time step. The overall efficiency of the implicit solution procedure depends on what kind of iteration solver is used. This will be discussed in the next section.

Iterative Solution of Algebraic Equations

Because the hydrodynamic problems are nonlinear, iterative solution methods are often used, especially for multidimensional problems. The simplest iteration methods are Jacobi method and Gauss-Seidel method. However, the convergence speed of these two methods is usually slow. To speed up the convergence, the Thomas algorithm and the Alternating Direction Implicit (ADI) iterative method have been widely used. Another iteration method of even faster convergence is the Strongly Implicit Procedure (SIP) proposed by Stone (1968). The idea is to approximately factorize the algebraic equations into two subsystems with a lower triangular matrix and an upper triangular matrix, and then solve the two subsystems separately by a direct method. Other iteration methods include Newton's method, Conjugate Gradient method, Biconjugate Gradients method, GMRES, multigrid method, etc. In addition, the relaxation method is often adopted to enhance the efficiency of iteration. Over- and under-relaxation methods can accelerate or slow down the convergence speed, but for nonlinear systems, such as hydrodynamic equations, under-relaxation is more often used.

Numerical Solutions of Free Surface Flow

For 1-D steady or quasi-steady flow model, the governing equation is the energy equation, which can be solved by the standard step method. For 1-D unsteady flow model, the most widely used numerical scheme is Preissmann's four-point implicit scheme. In a single channel or in a dendritic channel network, the resulting algebraic equations can be solved by applying the Thomas algorithm. For a looped channel network, the method proposed by Cunge et al. (1980) is suggested. The Preissman's scheme may encounter instability in the case of transcritical flow. Therefore, it is usually limited to subcritical flows. For the flow mixed with subcritical and supercritical regimes, the approximate Riemann solvers and TVD schemes are often used (Toro, 2001).

In the depth-averaged 2-D shallow water equations, Equations (11)-(13), the water depth appears in the continuity equation, providing a strong linkage between velocity and pressure (water level). Usually, upwind schemes are needed to discretize the convection terms in the momentum equations and even the spatial derivative terms in the continuity equations (i.e., upwinding flux). When the central difference scheme is used to discretize these terms, artificial dissipations or TVD limiters are often used to suppress the numerical oscillations. Some solution methods for the Navier-Stokes equations can be used for the 2-D shallow water equations. For example, the Rhie and Chow's (1983) momentum interpolation technique on non-staggered grid (Wu, 2004) and the correction-type methods on staggered or partially staggered grids (Jia and Wang, 1999) have been adopted to solve Equations (11)–(13).

In the full 3-D Navier-Stokes equations, Equations (1) and (2), the momentum equations link the velocity to the pressure gradient, but the continuity equation does not directly link to the pressure and is just an additional constraint on the velocity field. Owing to such a weak linkage, the convergence and stability of a numerical solution of the Navier-Stokes equations depend largely on how the pressure gradient and velocity in these equations are evaluated. Storing the variables at the geometric center of the control volume coupled with a linear

interpolation for inter-nodal variation usually leads to non-physical node-to-node oscillations. One approach to avoid such numerical oscillations is to use the staggered grid adopted in the MAC method, the projection method, and the SIMPLE algorithm. Another approach is to use the momentum interpolation technique proposed by Rhie and Chow (1983) based on the collocated (non-staggered) grid (Wu et al., 2000a).

In 3-D simulations of river flow, the computational domain is movable due to the free-surface and bed-surface variations. One approach to handle this problem is ignoring the free-surface variation and treating the free-surface as a rigid lid boundary. The location of the rigid lid can be estimated by a 1-D or 2-D model. This approach is simple but only applicable to a short reach where the water surface elevation varies gently. Another approach is the volume-tracking method, which uses a fixed grid, and defines the water surface profile through the volume of fluid at each grid cell. The MAC and VOF algorithms (Hirt and Nichols, 1981) are examples of this group. The third approach is the surface-tracking method, which uses the moving grid that follows the free-surface elevation change. At least one grid line is along the free surface so that the surface shape is approximately matched. In the surface-tracking method, the location of water surface is usually determined by the free-surface kinematic condition given by Equation (6), the depth-integrated continuity equation, Equation (11), or the 2-D Poisson equation derived by Wu et al. (2000a) from the 2-D depth-averaged momentum equations.

In the 3-D shallow water equations, Equations (3)–(5), the pressure (water level) field becomes a 2-D quantity, but the weak linkage between the pressure and velocity still exists. Therefore, most of the current 3-D shallow water flow models adopt the staggered grid. Taking advantage of the 2-D feature of the pressure, Sheng (1983) and others suggested the splitting of internal module and external module. The external module is the depth-averaged 2-D model, which handles the fast barotropic dynamics and computes the water level field. The internal module handles the slower baroclinic vertical flow structure by solving the 3-D equations. Casulli and Cheng (1992) proposed an algorithm that uses an implicit scheme in the vertical direction and a semi-implicit scheme in the horizontal direction. They derived a discrete 2-D Poisson equation to determine the water level. Wu and Lin (2011) developed an implicit finite-volume method to solve Equations (3)–(5) by using the SIMPLEC algorithm and the Rhie and Chow's (1983) momentum interpolation technique to handle the coupling of velocity and water level on a non-staggered quadtree rectangular mesh.

Numerical Solutions of Sediment Transport

Although the physical interactions between the water and sediment always exist, the majority of the early sediment transport models have decoupled the flow and sediment calculations. Recent research has found that the coupled model is more stable and more accurate in case of strong sediment transport (Holly and Rahuel, 1990; Cao et al., 2002). However, the nonlinearity of flow problem may reduce the efficiency of solving the flow and sediment transport equations simultaneously. In addition, the sediment in the vast majority of rivers has very low concentration, and the time scales of flow and channel morphodynamic processes can be significantly different, especially in the case where bed load is dominant. Therefore, fully coupling the flow and sediment transport are usually not cost-effective. Wu et al. (2004) and Wu (2004) adopted a “semi-coupling” procedure, in which the flow calculation is decoupled from sediment calculation, but the three components of the sediment

transport module: sediment transport, bed change, and bed material sorting are solved in a coupled fashion. This semi-coupling procedure has been found to be very stable and efficient computationally.

APPLICATION EXAMPLES

Three representative examples are presented to highlight the important capabilities of the NEST model. The first case is the application of the depth-averaged NEST model in the Lower Yellow River. The second case shows application of the depth-averaged 2-D model enhanced with dispersion terms for the sediment transport in a curved channel. The third case is calculation of local scour near bridge piers using a 3-D model with the sediment entrainment function considering the effects of local flow features. More examples can be found in Wu (2007) and other relevant references.

Case 1: Sediment Transport in the Lower Yellow River

Wu et al. (2006) simulated the flow and sediment transport in the lower Yellow River during the 1982 flood. The computational domain was the 103 km long reach between the Huayuankou and Jiahetan gauge stations. The Huayuankou station, located 259 km downstream of the Sanmenxia Dam, was set as the inlet. The computational mesh consisted of 201 and 21 points in the longitudinal and transverse directions, respectively, shown in Figure 3. The measured time series of flow discharge and sediment concentration at Huayuankou, shown in Figure 4(a), were used as inflow boundary conditions, while the measured time series of water stage at Jiahetan was used as the outlet boundary condition. The peak flow discharge of this flood at Huayuankou was $15,300 \text{ m}^3/\text{s}$, and the peak sediment concentration was 66.6 kg/m^3 . The sediment was non-uniform, with sizes ranging from 0.002 to 0.18 mm. Five size classes were used to represent the non-uniform sediment mixture. The Manning roughness coefficient was between 0.009 and 0.015, with bigger values for the rising stage and smaller values for the falling stage of the flood. The computational period was from July 30 to August 11, 1982. The time step was 15 minutes. The adaptation coefficient α was 0.25. The effect of sediment concentration was considered by modifying the settling velocity of sediment particles according to the Richardson-Zaki (1954) formula.

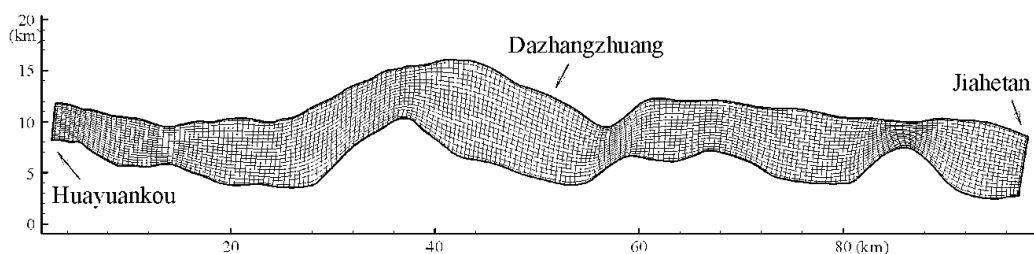


Figure 3. Computational mesh between Huayuankou and Jiahetan

Figure 4(b) shows the measured and simulated flow discharges and sediment concentrations at Jiahetan (outlet). The simulated results generally agree well with the

measured data. Because of deposition, the simulated peak sediment concentration at Jiahetan corresponding to the peak flow decreased to 45.57 kg/m^3 , compared to the measured value of 40.7 kg/m^3 . The time delay between peak flow and sediment concentration was 34.5 and 37.5 hr at the inlet and outlet, respectively, and exhibited an increasing trend downstream. Figure 5 shows the simulated flow field corresponding to a flow discharge of $4,000 \text{ m}^3/\text{s}$ at Huayuankou. The vectors represent the flow direction and magnitude, while the contours denote the flow depth. It can be seen that the main flow meandered in the river and interacted with the flow in floodplains.

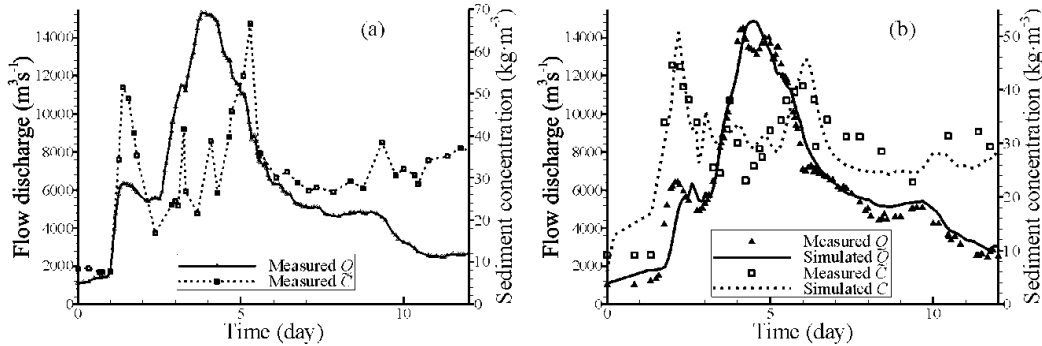


Figure 4. Flow discharges and sediment concentrations at (a) Huayuankou (Inlet) and (b) Jiahetan (Outlet) (Wu et al., 2006)

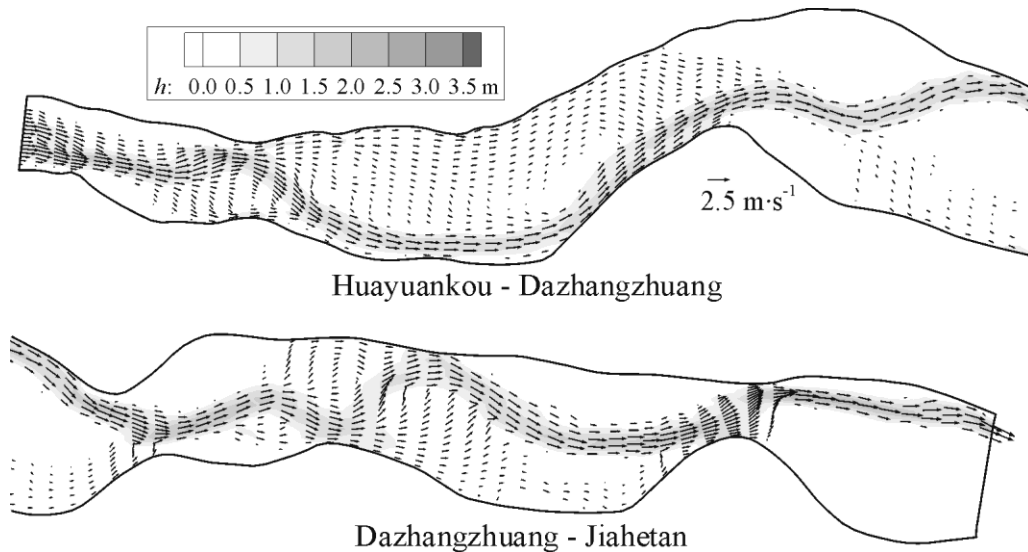


Figure 5. Simulated flow field at flow discharge of $4,000 \text{ m}^3\text{s}^{-1}$ at Huayuankou (Wu et al., 2006)

Case 2. Sediment Transport in a Channel Bend

Wu and Wang (2004) simulated the sediment transport and morphological change in an 180° bend under unsteady flow conditions, which were experimentally investigated by Yen

and Lee (1995). The width of the flume was 1 m, the radius of curvature at the centerline was 4 m, and the initial bed slope was 0.002. The flow hydrograph was triangular. The base flow discharge was $0.02 \text{ m}^3/\text{s}$, and the base flow depth, h_o , was 0.0544 m. In the simulated case (run 4), the peak flow discharge was $0.053 \text{ m}^3/\text{s}$, and the duration was 240 min. The peak of the hydrograph was set at the first third of its duration. The sediment was non-uniform and had a median diameter of 1.0 mm and a standard deviation of 2.5. The Manning roughness coefficient was given as $d_{50}^{1/6}/20$ in the simulation, with d_{50} being the median size of the bed material in the mixing layer. The two parameters in the helical flow intensity model, Equation (43), were set as $\lambda_t = 3.0$ and $\beta_t = 1.0$. The computational mesh in the bend reach consisted of 91 and 31 points in the longitudinal and transverse directions, respectively. The time step was 1 min. Figure 6 compares the measured and simulated bed change contours in the bend, and Figure 7 shows the lateral profiles of the bed changes at four cross-sections. The general patterns of the deeper channel along the outer wall and the point bar along the inner wall are reproduced well by the model. The calculated bed changes are in agreement with the measured data. Without considering the helical flow effect, one cannot obtain such reasonable results.

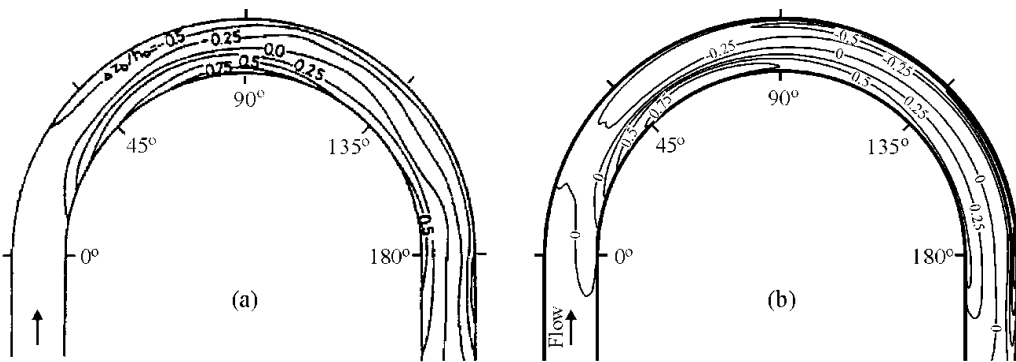


Figure 6. (a) Measured and (b) Calculated Bed Changes Contours (Wu and Wang, 2004)

Case 3: Local Scour around Bridge Piers

Wu (2007) simulated local scour process at bridge piers using the 3-D flow and sediment transport model published by Wu et al. (2000a) with modifications considering the effects of local flow features on sediment transport, as explained in the previous section. The model adopts the standard $k-\varepsilon$ turbulence model and uses the finite volume method on quadrilateral grid to discretize the governing equations. The computational mesh consisted of 43 and 25 points in the transverse and vertical directions, respectively, and a suitable number of points in the longitudinal direction depending on the flume length. The plan view of the mesh around a cylindrical pier is shown in Figure 8. The vertical grid spacing was refined near the bed. The sediment transport capacity was determined using the van Rijn formula modified with Equation (51). The sediment adaptation length was determined using $L = \min(0.4t, 7.3h_o)$, in which t is the elapsed time in hours and h_o is the approach flow depth in meters.

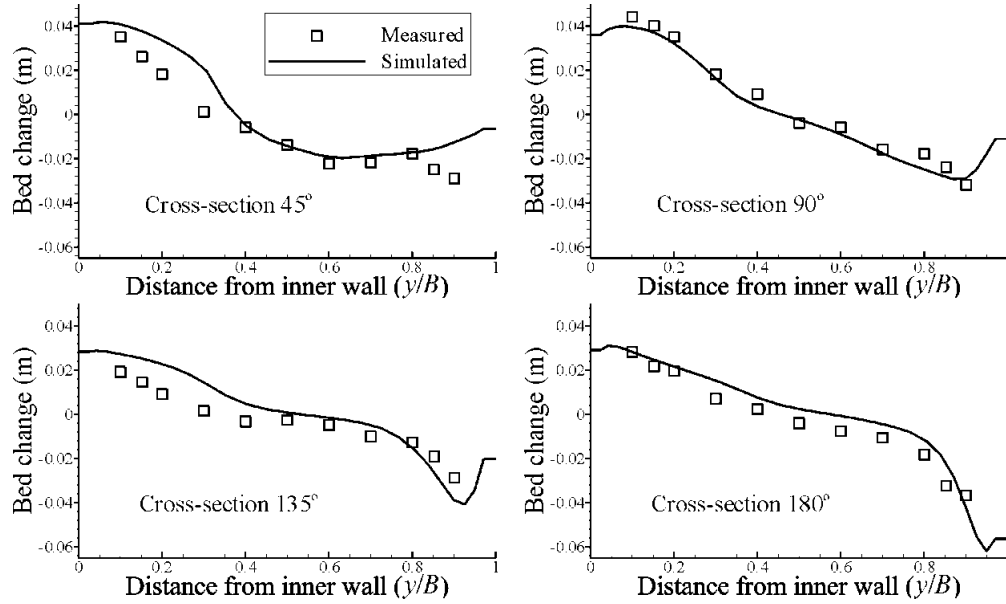


Figure 7. Measured and calculated bed changes at four cross-sections (Wu and Wang, 2004)

Figure 9 compares the simulated and measured scour holes at a cylindrical bridge pier for Yanmaz and Altinbilek's (1991) run 3 with a pier diameter (D) of 6.7 cm, a sediment size of 1.07 mm, a flow discharge of 30 l/s, and an approach flow depth of 0.135 m. The simulated scour depth contours in the hole agree well with the measured data. The simulation predicted deposition downstream of the scour hole, but the measurement lacked this information. Figure 10 compares the simulated and measured deepest scour depths varying with time for Yanmaz and Altinbilek's (1991) run 3, Ettema's (1980) experiment with $D = 0.24$ m and $d_{50} = 1.9$ mm, and the run 7 ($D = 0.91$ m, $d_{50} = 2.9$ mm) of Sheppard et al. (2004). Durations (t_e) of these three runs were 5, 14.5, and 188 hr, respectively. Erosion was very intensive at first and then reduced gradually. The erosion processes were reproduced well by the numerical model.

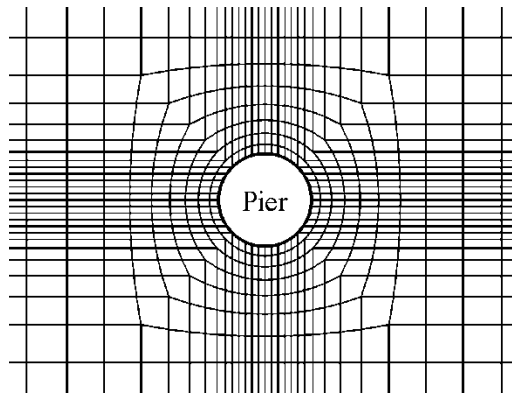


Figure 8. Computational mesh near a cylindrical pier (Plan View)

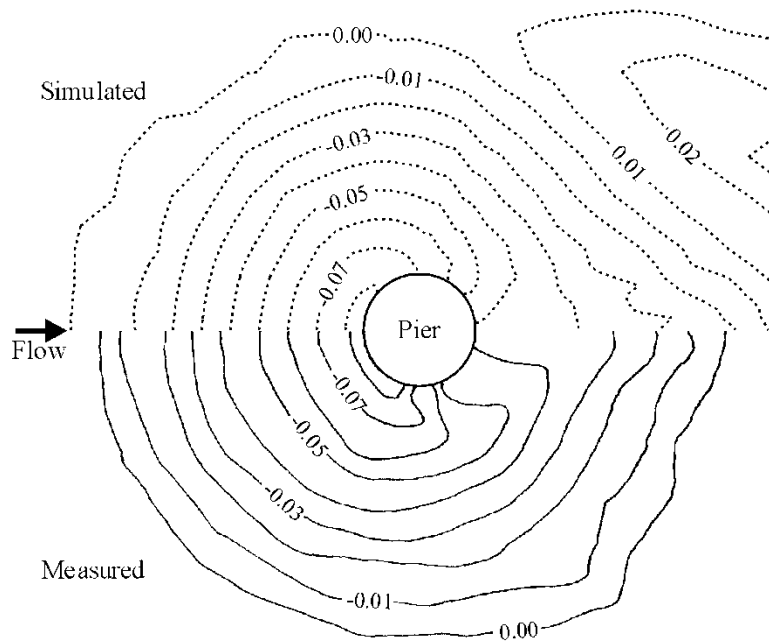


Figure 9. Measured and simulated scour depth contours (m) at a cylindrical pier (Yannmaz and Altinbilek's Run 3 at 100 min)

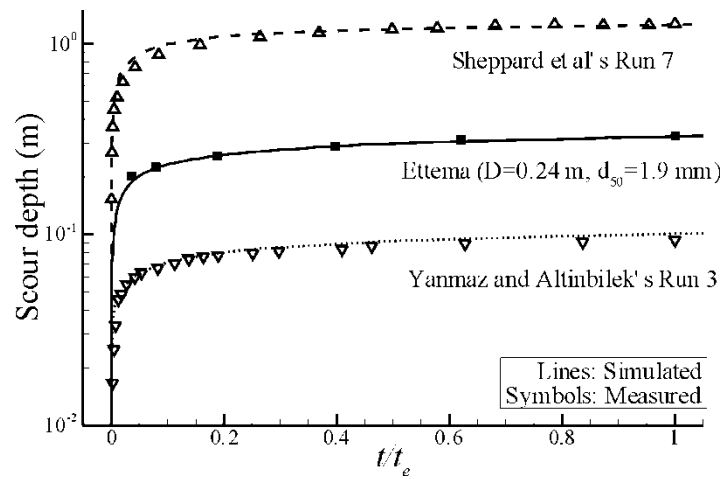


Figure 10. Temporal variation of the deepest scour depth at cylindrical piers

CONCLUSION

Under the assumption of low sediment concentration and slow bed change, the sediment-laden flow can be described using a clear water flow model with a decoupled sediment

transport model. In a 3-D model, the flow is governed by the 3-D Reynolds-averaged Navier-Stokes equations or their simplified form for the shallow water flow under hydrostatic pressure assumption. The suspended-load transport is governed by the traditional convection-diffusion equation with a sediment settling term.

By integrating the 3-D model equations over the flow depth (or cross-section), the depth-averaged 2-D (or 1-D) flow and suspended-load transport equations are derived, in which dispersion terms appear due to the non-uniformity of flow velocity and suspended-load concentration along the depth. The dispersion terms are often combined with the turbulent stress terms by introducing the mixing coefficient or effective eddy viscosity and sediment diffusivity, or combined with the convection terms by introducing flow momentum and sediment flux correction factors, or evaluated using analytical models for the vertical profiles of secondary flow velocity and suspended-load concentration. The depth-averaged suspended-load transport equation has a source term due to exchange between suspended load and bed load (or bed material). It is modeled by relating the actual and capacity (equilibrium) near-bed sediment concentrations to the depth-averaged values via the adaptation coefficient α . In addition, the depth-averaged velocity of suspended load is found to be smaller than the depth-averaged flow velocity, and this lag is considered through introducing the correction factor β_s in the storage term in the depth-averaged suspended-load transport equation. For fine sediments, β_s is close to 1.0, but for coarse sediments β_s is approximately between 0.4–1.0 depending on the Rouse number and Chezy coefficient.

The bed-load transport equation is derived by integrating the 3-D sediment transport equation over the bed-load layer. The equation has source terms to account for exchanges between suspended load and bed load and between bed load and bed material. By defining the bed change as contributions from bed load and suspended load, the bed-load transport equation is closed, in which sediment adaptation length L and bed-load velocity u_b are the parameters to be modeled. The bed-load velocity is determined using an empirical formula. It usually is slower than flow velocity, so that the lag between bed-load and flow is taken into account in the model. The derived bed-load transport equation can be used in both 3-D and depth-averaged 2-D models. Laterally integrating it leads to the section-averaged 1-D bed-load transport equation.

The derived suspended-load and bed-load transport equations are the basic equations of the sediment transport model that separates moving sediments into suspended load and bed load. An alternative approach is to add the suspended-load and bed-load transport equations to derive the bed-material load (or total load) transport equation in the depth-averaged 2-D or 1-D model. This bed-material load modeling approach solves one less differential equation for each sediment size class and is computationally more efficient than the suspended-load and bed-load separation approach. Moreover, the two parameters, adaptation coefficient α and adaptation length L , in the separation method are combined in the bed-material load model into a single parameter, either as the adaptation coefficient α_l or the adaptation length L_l .

Methods and guidance have been developed for evaluating sediment adaptation length and coefficient. Unfortunately, these parameters are empirical and depend on the flow and sediment conditions and domain geometric characteristics. The suspended-load adaptation coefficient α can be determined using several semi-empirical formulas, which are developed

with certain simplifications and assumptions and usually give values larger than 1.0 for α . In practice, α is found to have values less than 1.0 (mostly between 0.25-1.0) in 1-D models. The bed-load adaptation length L_b is related to scales of sediment transport and bed forms. Because α and L_b are affected by many complex factors, the most reliable way is to calibrate them using measured data for specific cases.

The sediment transport capacity is another important parameter in the sediment transport model. It includes the depth-averaged capacity concentration of suspended load in the depth-averaged 2-D and 1-D models, the near-bed capacity concentration of suspended load in the 3-D model, and the capacity transport rate of bed load in all 1-D, 2-D and 3-D models. Dozens of empirical formulas are available in the literature to determine the sediment transport capacity. Recommendations are provided for selection of these formulas. However, calibration using measurement data is always the most reliable way.

In the case of non-uniform sediment transport, the sediment mixture is divided into multiple size classes and the aforementioned transport equations are applied to each sediment size class. The hiding and exposure mechanism in the non-uniform bed materials is taken into account through the correction factors introduced in the sediment incipient motion and sediment transport capacity formulas. The bed material is often divided into multiple layers in depth, and the mixing layer at the bed surface is facilitated to exchange with moving sediments. The sediment sorting equation in the mixing layer is derived according to mass conservation.

Additionally, turbulence closure, bed roughness, dispersion in curved channel, sediment transport over steep slope, sediment entrainment near in-stream structures, and bank erosion are briefly discussed, to close and enhance the flow and sediment transport model. The numerical methods often used to solve the flow and sediment transport equations are briefly summarized, including numerical discretization methods, iterative solution of algebraic equations, coupling of velocity and pressure in the flow equations, and decoupling and coupling of flow and sediment calculations.

Three test cases are selected to demonstrate the capabilities of the NEST model to take into account the lag of flow and sediment transport in an alluvial river reach, the effects of helical flow on the main flow, sediment transport and channel morphology in a channel bend by incorporating the momentum and flux dispersions, and the local scour near a bridge pier by enhancing the formula of sediment entrainment affected by the 3-D local flow features. More cases can be found in the relevant publications.

ACKNOWLEDGEMENTS

This study was part of the research project sponsored by the USDA-ARS Specific Research Agreement No. 58-6408-7-236 (monitored by the USDA-ARS National Sedimentation Laboratory) and The University of Mississippi.

REFERENCES

- Ackers, P., White, W.R., (1973). Sediment transport: A new approach and analysis. *Journal of the Hydraulics Division*, ASCE, 99(HY11), 2041–2060.
- Armanini, A., Di Silvio, G., (1988). A one-dimensional model for the transport of a sediment mixture in non-equilibrium conditions. *Journal of Hydraulic Research*, IAHR, 26(3), 275–292.
- Arulanandan, K., Gillogley, E., Tully, R., (1980). Development of a quantitative method to predict critical shear stress and rate of erosion of naturally undisturbed cohesive soils. Report GL-80-5, U.S. Army Engineers Waterway Experiment Station, Vicksburg, Mississippi, USA.
- Ashida, K., Michiue, M., (1971). An investigation of river bed degradation downstream of a dam. Proc. 14th Congress of IAHR, Paris, France, 3, 247–256.
- Bell, S.G., Sutherland, A.J., (1983). Non-equilibrium bed load transport by steady flows. *Journal of Hydraulic Engineering*, 109(3), 353–367.
- Bridge, J.S., Dominic, D.F., (1984). Bed load grain velocities and sediment transport rates. *Water Resources Research*, 20(4), 476–490.
- Brooks, N.H., (1963). Discussion of boundary shear stresses in curved trapezoidal channels by A.T. Ippen and P.A. Drinker. *Journal of the Hydraulics Division*, ASCE, 89(HY3), 327–333.
- Brownlie, W.R., (1981). Compilation of fluvial channel data: Laboratory and field. Report No. KH-R-43B, W.M. Keck Laboratory of Hydraulics and Water Resources, California Institute of Technology, Pasadena, Calif., USA
- Cao, Z., Day, R., Egashira, S., (2002). Coupled and decoupled numerical modeling of flow and morphological evolution in alluvial rivers. *Journal of Hydraulic Engineering*, ASCE, 128(3), 306–321.
- Casulli, V., Cheng, R.T., (1992). Semi-implicit finite difference methods for three-dimensional shallow water flow. *International Journal of Numerical Methods in Fluids*, 15(6), 629–648.
- Cheng, N.S., (2004). Analysis of velocity lag in sediment-laden open channels flows. *Journal of Hydraulic Engineering*, ASCE, 130(7), 657–666.
- Cunge, J.A., Holly, F.M.Jr., Verwey, A., (1980). Practical aspects of computational river hydraulics. Pitman Publishing Inc., Boston, MA, USA.
- Daubert, A., Lebreton, J.C., (1967). Etude experimentale et sur modele mathematique de quelques aspects des processus d'erosion des lits alluvionnaires, en regime permanent et non permanent. Proc. 12th IAHR Congress, 3, Fort Collins, USA.
- Day, T.J., (1980). A study of the transport of graded sediments. Report No. IT 190, HR Wallingford, U. K.
- De Vriend, H.J., (1981). Steady flow in shallow channel bends. Communications on Hydraulics, 81-3, Delft University of Technology, Delft, The Netherlands.
- Dou, G.R., (1963). Sediment transport theory. Nanjing Hydraulic Research Institute, China (in Chinese).
- Duan, J.G., Wang, S.S.Y., Jia, Y., (2001). The application of the enhanced CCHE2D model to study the alluvial channel migration processes. *Journal of Hydraulic Research*, IAHR, 39(5), 469–480.
- Egiazaroff, I.V., (1965). Calculation of nonuniform sediment concentration. *Journal of the Hydraulics Division*, ASCE, 91(HY4), 225–247.

- Einstein, H.A., (1950). The bed-load function for sediment transportation in open channel flows. Technical Bulletin No. 1026, U.S. Department of Agriculture, Soil Conservation Service, Washington D.C., USA.
- Einstein, H.A., Barbarossa, N.L., (1952). River channel roughness. *Transactions of American Society of Civil Engineers*, 117, 1121–1146.
- Engelund, F., (1974). Flow bed topography in channel bend. *Journal of the Hydraulics Division*, ASCE, 100(11), 1631–1648.
- Engelund, F., Hansen, E., (1967). A monograph on sediment transport in alluvial streams. Teknisk Forlag, Copenhagen, Denmark.
- Ettema, R., (1980). Scour at bridge piers. University of Auckland, New Zealand.
- Fang, H.W., (2003). Case studies of three-dimensional numerical simulation for total sediment transport. *International Journal of Sediment Research*, 18(2), 158–165.
- Flokstra, C., (1977). The closure problem for depth-average two dimensional flow. Publication No. 190, Delft Hydraulics Laboratory, The Netherlands.
- Francis, J.R.D., (1973). Experiments on the motion of solitary grains along the bed of water stream. *Proceedings The Royal Society London*, Ser. A, 332(1591), 443–471.
- Garbrecht, J., Kuhnle, R., Alonso, C., (1995). A sediment transport capacity formulation for application to large channel networks. *Journal of Soil and Water Conservation*, 50(5), 527–529.
- Garcia, M., Parker, G., (1991). Entrainment of bed sediment into suspension. *Journal of Hydraulic Engineering*, ASCE, 117(4), 414–433.
- Greimann, B.P., Holly, F.M., (2001). Two-phase flow analysis of concentration profiles. *Journal of Hydraulic Engineering*, ASCE, 127(9), 753–762.
- Han, Q.W., (1980). A study on the nonequilibrium transportation of suspended load. Proc. First International Symposium on River Sedimentation, Beijing, China.
- Hayashi, T.S., Ozaki, Ichibashi, T., (1980). Study on bed load transport of sediment mixture. Proc. 24th Japanese Conference on Hydraulics, Japan.
- Hirt, C.W., Nichols, B.D., (1981). Volume of fluid (VOF) method for dynamics of free boundaries. *Journal of Computational Physics*, 39, 201–221.
- Holly, F.M., Rahuel, J.L., (1990). New numerical/physical framework for mobile-bed modeling, Part I: Numerical and physical principles. *Journal of Hydraulic Research*, IAHR, 28(4), 401–416.
- Jankowski, J.A., Malcherek, A., Zielke, W., (1994). Numerical modeling of sediment transport processes caused by deep sea mining discharge. Proc. the OCEANS 94 Conference, Brest, IEEE/SEE, 3, 269–276.
- Jia, Y., Kitamura, T., Wang, S.S.Y., (2001). Simulation of scour process in plunging pool of loose bed-material. *Journal of Hydraulic Engineering*, ASCE, 127(3), 219–229.
- Jia, Y., Wang, S.S.Y., (1999). Numerical model for channel flow and morphological change studies. *Journal of Hydraulic Engineering*, ASCE, 125(9), 924–933.
- Jin, Y.C., Steffler, P.M., (1993). Predicting flow in curved open channels by depth-averaged method. *Journal of Hydraulic Engineering*, ASCE, 119(1), 109–124.
- Karim, F., Kennedy, J.F., (1982). IALLUVIAL: A computer-based flow- and sediment-routing model for alluvial streams and its application to the Missouri River. Technical Report No. 250, Iowa Institute of Hydraulic Research, University of Iowa, USA.
- Lee, H.Y., Hsu, I.S., (1994). Investigation of saltating particle motions. *Journal of Hydraulic Engineering*, ASCE, 120(7), 831–845.

- Leonard, B.P., (1979). A stable and accurate convective modelling procedure based on quadratic interpolation. *Computer Methods in Applied Mechanics and Engineering*, 19(1), 59–98.
- Luque, R.F., van Beek, R., (1976). Erosion and transport of bed-load sediment. *Journal of Hydraulic Research*, IAHR, 14(2), 127–144.
- Meyer-Peter, E., Mueller, R., (1948). Formulas for bed-load transport. Report on Second Meeting of IAHR, Stockholm, Sweden, 39–64.
- Muste, M., Patel, V.C., (1997). Velocity profiles for particles and liquid in open-channel flow with suspended sediment. *Journal of Hydraulic Engineering*, ASCE, 123(9), 742–751.
- Nakagawa, H., Tsujimoto, T., (1980). Sand bed instability due to bed load motion. *Journal of the Hydraulics Division*, ASCE, 106(12), 2029–2051.
- Odgaard, A.J., (1981). Transverse bed slope in alluvial channels bends. *Journal of the Hydraulics Division*, ASCE, 107(12), 1677–1694.
- Osman, A.M., Thorne, C.R., (1988). Riverbank stability analysis, I: Theory. *Journal of Hydraulic Engineering*, ASCE, 114(2), 134–150.
- Parker, G., Kilingeman, P.C., McLean, D.G., (1982). Bed load and size distribution in paved gravel-bed streams. *Journal of the Hydraulics Division*, ASCE, 108(4), 544–571.
- Phillips, B.C., Sutherland, A.J., (1989). Spatial lag effects in bed load sediment transport. *Journal of Hydraulic Research*, IAHR, 27(1), 115–133.
- Proffit, G.T., Sutherland, A.J., (1983). Transport of nonuniform sediment. *Journal of Hydraulic Research*, IAHR, 21(1), 33–43.
- Rahuel, J.L., Holly, F.M., Chollet, J.P., Belleudy, P.J., Yang, G., (1989). Modeling of riverbed evolution for bedload sediment mixtures. *Journal of Hydraulic Engineering*, ASCE, 115(11), 1521–1542.
- Rhie, C.M., Chow, W.L., (1983). Numerical study of the turbulent flow past an airfoil with trailing edge separation. *AIAA Journal*, 21(11), 1525–1532.
- Ribberink, J.S., Blom, A., van der Sheer, P., (2002). Multi-fraction techniques for sediment transport and morphological modeling in sand-gravel rivers. River Flow 2002, Bousmar and Zech (eds.), Swets & Zeitinger, Lisse, 731–739.
- Richardson, J.F., Zaki, W.N., (1954). Sedimentation and fluidisation, Part I. *Transactions of the Institution of Chemical Engineers*, 32(1), 35–53.
- Rodi, W., (1993). Turbulence models and their application in hydraulics. 3rd Edition, IAHR Monograph, Balkema, Rotterdam.
- Rozovskii, I.L., (1957). Flow of water in bends of open channel. Academy of Sciences of the Ukrainian SSR, Kiev.
- Sekine, M., Parker, G., (1992). Bed-load transport on transverse slope, I. *Journal of Hydraulic Engineering*, ASCE, 118(4), 513–535.
- Sheng, Y.P., (1983). Mathematical modeling of three-dimensional coastal currents and sediment dispersion: Model development and application. Technical Report CERC-83-2, Aeronautical Research Associates of Princeton, Inc., N.J., USA.
- Sheppard, D.M., Odeh, M., Glasser, T., (2004). Large scale clear-water local pier scour experiments. *Journal of Hydraulic Engineering*, ASCE, 130(10), 957–963.
- Simon, A., Curini, A., Darby, S.E., Langendoen, E.J., (2000). Bank and near-bank processes in an incised channel. *Geomorphology*, 35, 193–217.

- Spalding, D.B., (1972). A novel finite-difference formulation for differential expressions involving both first and second derivatives. *International Journal for Numerical Methods in Engineering*, 4(4), 551–559.
- Spasojevic, M., Holly, F.M.Jr., (1993). Three-dimensional numerical simulation of mobile-bed hydrodynamics. Technical Report No. 367, Iowa Institute of Hydraulic Research, The University of Iowa, USA.
- Stone, H.L., (1968). Iterative solution of implicit approximation of multidimensional partial differential equations. *SIAM Journal on Numerical Analysis*, 5(3), 530–558.
- Thomas, W.A., (1982). Chapter 18: Mathematical modeling of sediment movement. Gravel-bed rivers, R.D. Hey et al., eds., John Wiley & Sons, Ltd., New York, USA.
- Thuc, T., (1991). Two-dimensional morphological computations near hydraulic structures. Doctoral Dissertation, Asian Institute of Technology, Bangkok, Thailand.
- Toro, E.F., (2001). Shock-capturing methods for free-surface shallow flows. Wiley.
- van Rijn, L.C., (1984a). Sediment transport, Part I: Bed load transport. *Journal of Hydraulic Engineering*, ASCE, 110(10), 1431–1456.
- van Rijn, L.C., (1984b). Sediment transport, Part II: Suspended load transport. *Journal of Hydraulic Engineering*, ASCE, 110(11), 1613–1641.
- van Rijn, L.C., (1984c). Sediment transport, Part III: Bed forms and alluvial roughness. *Journal of Hydraulic Engineering*, ASCE, 110(12), 1733–1754.
- van Rijn, L.C., (1989). Handbook: Sediment transport by current and waves. Report H 461, Delft Hydraulics, The Netherlands.
- Wang, S.S.Y., Adeff, S.E., (1986). Three-dimensional modeling of river sedimentation processes. Proc. of the 3rd International Symposium on River Sedimentation, The University of Mississippi, USA.
- Wang, S.S.Y., Hu, K.K., (1992). Improved methodology for formatting finite element hydrodynamic models. Finite Element in Fluids, T.J. Chung (ed.), Hemisphere Publishing Corp., 8, 457–478.
- Wellington, N.W., (1978). A sediment-routing model for alluvial streams. MS Thesis, University of Melbourne, Australia.
- Wu, W., (1991). The study and application of 1-D, horizontal 2-D and their nesting mathematical models for sediment transport. Ph.D. Dissertation, Wuhan University of Hydraulic and Electric Eng., Wuhan, China (in Chinese).
- Wu, W., (2004). Depth-averaged 2-D numerical modeling of unsteady flow and nonuniform sediment transport in open channels. *Journal of Hydraulic Engineering*, ASCE, 130(10), 1013–1024.
- Wu, W., (2007). Computational river dynamics. Taylor & Francis, London, U.K.; Balkema, Leiden, The Netherlands.
- Wu, W., Altinakar, M., Wang, S.S.Y., (2006). Depth-average analysis of hysteresis between flow and sediment transport under unsteady conditions. *International Journal of Sediment Research*, 21(2), 101–112.
- Wu, W., Lin, Q., (2011). An implicit 3-D finite-volume coastal hydrodynamic model. Proc. 7th Int. Symposium on River, Coastal and Estuarine Morphodynamics, September 6–8, Beijing, China.
- Wu, W., Marsooli, R., He, Z., (2012). A depth-averaged two-dimensional model of unsteady flow and sediment transport due to non-cohesive embankment break/breaching. *Journal of Hydraulic Engineering*, ASCE, 138(6), 503–516.

- Wu, W., Rodi, W., Wenka, T., (2000a). 3-D numerical modeling of water flow and sediment transport in open channels. *Journal of Hydraulic Engineering*, ASCE, 126(1), 4–15.
- Wu, W., Vieira, D.A., Wang S.S.Y., (2004). A 1-D numerical model for nonuniform sediment transport under unsteady flows in channel networks. *Journal of Hydraulic Engineering*, ASCE, 130(9), 914–923.
- Wu, W., Wang, S.S.Y., (1999). Movable bed roughness in alluvial rivers. *Journal of Hydraulic Engineering*, ASCE, 125(12), 1309–1312.
- Wu, W., Wang, S.S.Y., (2000). Mathematical models for liquid-solid two-phase flow. *International Journal of Sediment Research*, 15(3), 288–298.
- Wu, W., Wang, S.S.Y., (2003). Selection and evaluation of nonuniform sediment transport formulas for river modeling. XXX IAHR Congress, Thessaloniki, Greece.
- Wu, W., Wang, S.S.Y., (2004). Depth-averaged 2-D calculation of flow and sediment transport in curved channels. *International Journal of Sediment Research*, 19(4), 241–257.
- Wu, W., Wang, S.S.Y., Jia, Y., (2000b). Nonuniform sediment transport in alluvial rivers. *Journal of Hydraulic Research*, IAHR, 38(6), 427–434.
- Yalin, M.S., (1972). *Mechanics of Sediment Transport*. Pergamon Press.
- Yang, C.T., (1973). Incipient motion and sediment transport. *Journal of the Hydraulics Division*, ASCE, 99(HY10), 1679–1704.
- Yang, C.T., Wan, S., (1991). Comparisons of selected bed-material load formulas. *Journal of Hydraulic Engineering*, ASCE, 117(8), 973–989.
- Yanmaz, A.M., Altinbilek, H.D., (1991). Study of time-dependent local scour around bridge piers. *Journal of Hydraulic Engineering*, ASCE, 117(10), 1247–1268.
- Yen, C.L., Lee, K.T., (1995). Bed topography and sediment sorting in channel bend with unsteady flow. *Journal of Hydraulic Engineering*, ASCE, 121(8), 591–599.
- Zhang, R.J., (1961). *River dynamics*. Industry Press, Beijing, China (in Chinese).
- Zhang, R.J., Xie, J.H., (1993). *Sedimentation research in China, systematic selections*. China Water and Power Press, Beijing, China.
- Zhou, J., Lin, B., (1998). One-dimensional mathematical model for suspended sediment by lateral integration. *Journal of Hydraulic Engineering*, ASCE, 124(7), 712–717.
- Zhu, J. (1991). A low diffusive and oscillation-free convection scheme. *Communication in Applied Numerical Methods*, 7, 225–232.
- Zyserman, J.A., Fredsøe, J., (1994). Data analysis of bed concentration of suspended sediment. *Journal of Hydraulic Engineering*, ASCE, 120(9), 1021–1042.